High-resolution crystal structures of ribosome-bound chloramphenicol and erythromycin provide the ultimate basis for their competition

MAXIM S. SVETLOV,[1,5] ELENA PLESSA,[2,5] CHIH-WEI CHEN,[3] ANTHONY BOUGAS,[2] MARIOS G. KROKIDIS,[2] GEORGE P. DINOS,[2] and YURY S. POLIKANOV[1,3,4]

[1]Center for Biomolecular Sciences, University of Illinois at Chicago, Chicago, Illinois 60607, USA
[2]Department of Biochemistry, School of Medicine, University of Patras, 26504 Patras, Greece
[3]Department of Biological Sciences, University of Illinois at Chicago, Chicago, Illinois 60607, USA
[4]Department of Medicinal Chemistry and Pharmacognosy, University of Illinois at Chicago, Chicago, Illinois 60607, USA

ABSTRACT

The 70S ribosome is a major target for antibacterial drugs. Two of the classical antibiotics, chloramphenicol (CHL) and erythromycin (ERY), competitively bind to adjacent but separate sites on the bacterial ribosome: the catalytic peptidyl transferase center (PTC) and the nascent polypeptide exit tunnel (NPET), respectively. The previously reported competitive binding of CHL and ERY might be due either to a direct collision of the two drugs on the ribosome or due to a drug-induced allosteric effect. Because of the resolution limitations, the available structures of these antibiotics in complex with bacterial ribosomes do not allow us to discriminate between these two possible mechanisms. In this work, we have obtained two crystal structures of CHL and ERY in complex with the *Thermus thermophilus* 70S ribosome at a higher resolution (2.65 and 2.89 Å, respectively) allowing unambiguous placement of the drugs in the electron density maps. Our structures provide evidence of the direct collision of CHL and ERY on the ribosome, which rationalizes the observed competition between the two drugs.

Keywords: chloramphenicol; erythromycin; competition; antibiotic; 70S ribosome; X-ray structure; inhibition of translation; peptidyl transferase center; nascent peptide exit tunnel

INTRODUCTION

Protein synthesis is a key step in the gene expression pathway, which is catalyzed by the ribosome. The ribosome is composed of two unequal subunits, small and large (30S and 50S in bacteria), which join together to form a 70S particle. While the 30S subunit is in charge of decoding of the genetic information carried by the messenger RNA (mRNA), the peptidyl transferase center (PTC) of the 50S subunit links amino acids into a nascent polypeptide which is then threaded through the nascent peptide exit tunnel (NPET) that spans the body of the large subunit. PTC and NPET are the sites targeted by the broadest array of inhibitors belonging to several distinct chemical classes, including phenicols, lincosamides, oxazolidinones, pleuromutilins, streptogramins A and B, macrolides, and ketolides (Lin et al. 2018; Polikanov et al. 2018). Some of these inhibitors are among the most successful antimicrobial drugs used in the clinic to treat human bacterial infections (Van Boeckel et al. 2014).

Among the "oldest" and the best studied ribosome-targeting antibiotics are chloramphenicol (CHL, Fig. 1A) and erythromycin (ERY, Fig. 1B), which are also the prototype representatives of their respective chemical classes—phenicols and macrolides. CHL binds in the A site of the PTC and is thought to act as a competitive inhibitor, which prevents binding of an aminoacyl moiety of an incoming aminoacyl-tRNA substrate in the ribosomal A site resulting in inhibition of peptide bond formation (Hansen et al. 2003; Bulkley et al. 2010; Dunkle et al. 2010). Although the binding site of ERY (and all other macrolides) is located in the NPET 10 Å away from the PTC (Tu et al. 2005; Bulkley

[5]These authors contributed equally to this work.

Corresponding authors: dinosg@upatras.gr, yuryp@uic.edu

Article is online at http://www.rnajournal.org/cgi/doi/10.1261/rna.069260.118.

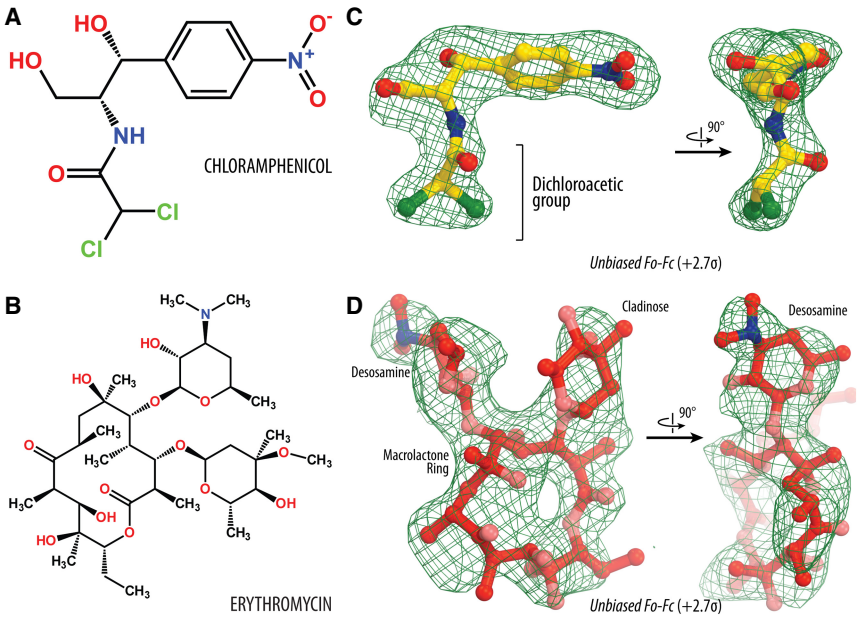

FIGURE 1. Electron density maps of ribosome-bound chloramphenicol and erythromycin. (*A*,*B*) Chemical structures of PTC-targeting antibiotic chloramphenicol (*A*, CHL) and NPET-binding macrolide erythromycin (*B*, ERY). (*C*,*D*) Unbiased F_o–F_c electron difference Fourier maps (green mesh) of CHL (*C*) and ERY (*D*) in complex with the *T. thermophilus* 70S ribosome viewed from two different perspectives. The refined models of CHL or ERY are displayed in their respective electron densities contoured at 2.7σ. Carbon atoms are colored yellow for CHL and red for ERY; nitrogens are blue; oxygens are red for CHL and salmon for ERY. Key chemical moieties of each drug are labeled.

et al. 2010; Dunkle et al. 2010), CHL and ERY are known to compete with each other (Vazquez 1966). This competition might be due to either a direct collision of the two drugs on the ribosome or a drug-induced allosteric effect. The early X-ray crystal structures of CHL and ERY in complex with the 50S large ribosomal subunit from eubacterium *Deinococcus radiodurans* (PDB entries 1K01 and 1JZY, respectively [Schlünzen et al. 2001]) suggested that these drugs have nonoverlapping binding sites (Supplemental Fig. S1A) and, therefore, should not directly compete with each other pointing to an allosteric mechanism. Later structures by two independent groups revealed substantially different orientations of CHL and ERY in their binding sites on the ribosome (Supplemental Fig. S1B,C; Bulkley et al. 2010; Dunkle et al. 2010). These structures of CHL and ERY in complex with bacterial 70S ribosomes from either *Escherichia coli* (*Eco*) (Dunkle et al. 2010) or *Thermus thermophilus* (*Tth*) (Bulkley et al. 2010) provided better quality maps allowing more accurate placement of the drugs in their binding sites. The structures revealed that the dichloroacetic moiety of CHL and the desosamine moiety of ERY, chemical groups that are crucial for binding to the ribosome, are either directly juxtaposed or potentially even overlap (Supplemental Fig. S1B,C; Bulkley et al. 2010; Dunkle et al. 2010). Whether the dichloroacetic moiety of CHL clashes with the desosamine of ERY depends on its particular orientation. However, even with the overall better quality crystallographic data, neither of the newer structures allowed for the unambiguous placing of the dichloroacetic moiety of CHL in the electron density maps. Nevertheless, these structures did not reveal any significant drug-induced rearrangements of the 23S rRNA nucleotides surrounding the PTC and NPET that would affect binding of the competitor drug. Therefore, most likely, the observed competition between the CHL and ERY is due to their steric hindrance.

In this work, we have obtained two crystal structures of CHL and ERY in complex with the *Tth* 70S ribosome at a higher resolution (2.65 and 2.89 Å, respectively) allowing unambiguous placement of the CHL dichloroacetic moiety and the ERY desosamine sugar. Our structures provide evidence of the direct collision of CHL and ERY on the ribosome, which rationalizes the observed competition between the two drugs.

RESULTS AND DISCUSSION

High-resolution structures of the ribosome-bound CHL and ERY

In order to unambiguously determine the exact location of all chemical moieties of CHL and ERY in their binding sites on the bacterial ribosome, we cocrystallized *Tth* 70S ribosomes in the presence of mRNA, deacylated A-, P-, and E-site tRNAs, and either CHL or ERY and solved the structures of the obtained complexes at 2.65 and 2.89 Å resolution, respectively (Supplemental Table S1). To our knowledge, these are the highest resolution structures of ribosome-bound CHL and ERY reported to date. Our structural data revealed more characteristic features of the drug molecules in the electron density maps (Figs. 1C,D, 2C,F). The better quality electron density maps allowed us to visualize the dichloroacetic moiety of CHL (Fig. 2C) and the desosamine sugar of ERY (Fig. 2F), whose placement in the previous structures was ambiguous (Fig. 2A,B,D,E). We believe that the optimized experimental procedures and inclusion of mRNA and tRNAs in our ribosome complexes provided additional stabilization to the ribosome that, in turn, contributed to the higher resolution, similar to other recent structures of ribosome-bound antibiotics (Almutairi et al. 2017; Metelev et al. 2017;

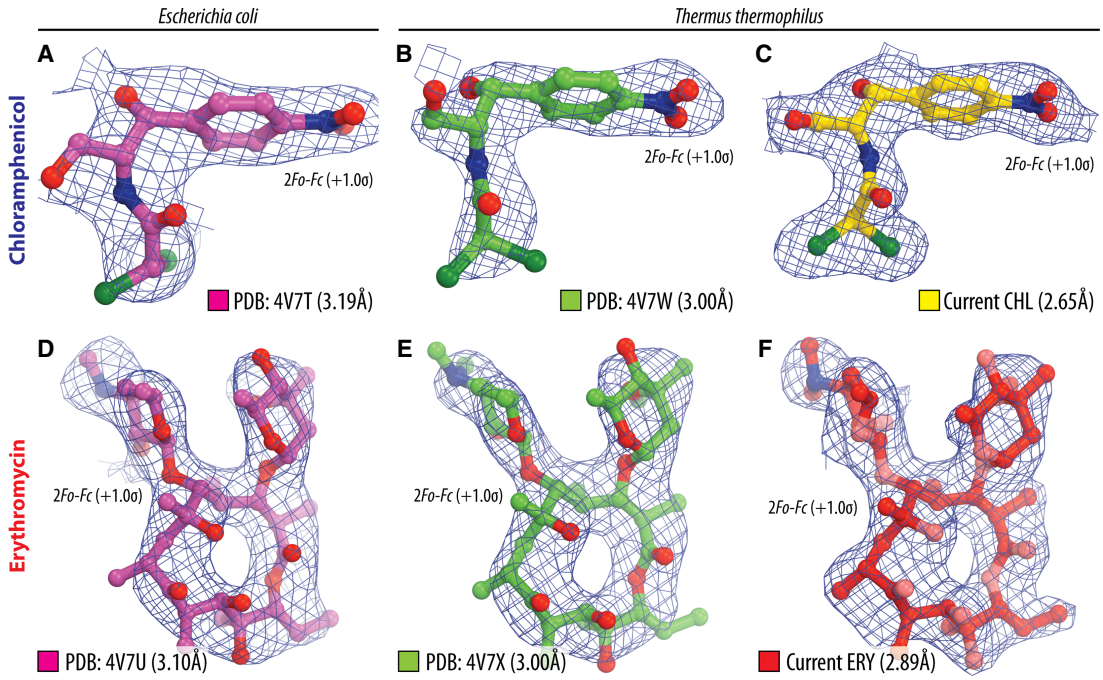

FIGURE 2. Comparison of the electron density maps of ribosome-bound CHL and ERY from different structures. The refined models of CHL (*A–C*) or ERY (*D–F*) that were either published previously (Bulkley et al. 2010; Dunkle et al. 2010) or determined in the current study are shown in their respective $2F_o–F_c$ electron density maps contoured at 1.0σ.

Osterman et al. 2017; Pantel et al. 2018; Tereshchenkov et al. 2018).

The binding position of the amphenicol moiety (but not the dichloracetic) of CHL molecule in our structure is identical to those observed previously for CHL bound to vacant 70S ribosomes from *Eco* (Supplemental Fig. S1B,D; Dunkle et al. 2010) or *Tth* (Supplemental Fig. S1C,D; Bulkley et al. 2010) in the absence of mRNA and tRNAs. This suggests that the presence of the deacylated tRNAs in the A and P sites does not affect the general mode of CHL binding to the ribosome. In our structure, the oxygens of the nitro group in the CHL form hydrogen bonds (H-bonds) with the A76 ribose 3′-hydroxyl of the deacylated A-site tRNA and A76 ribose 2′-hydroxyl of the deacylated P-site tRNA (Supplemental Fig. S2). It is unclear whether such interactions are possible in the translating ribosome when the A- and P-site tRNAs are attached to the aminoacyl and peptidyl groups, respectively. Nevertheless, our structure demonstrates that the amphenicol part of CHL anchors it in the PTC, directing the attached dichloroacetic moiety toward the macrolide binding site in the NPET. The overall quality of the obtained electron density map allowed us to unambiguously place all atoms of the dichloracetic moiety (Figs. 1C, 2C). Although in solution this moiety has a certain degree of rotational freedom, in the structure it adopts a unique conformation due to stabilization provided by the H-bond formed with the *N6* atom of nucleotide A2062 of the 23S rRNA, which rotates by ~160° around its N-glycosidic bond into a position where it forms a Hoogsteen base pair with the residue m^2A2503 (Fig. 3; Supplemental Movie S1). Similar reorientation of this nucleotide was previously observed in the 70S-CHL structures with vacant *Eco* (Dunkle et al. 2010) or *Tth* (Bulkley et al. 2010) ribosomes.

In our 70S-ERY structure, the drug molecule is located in the canonical macrolide-binding pocket in the NPET near the PTC, which is identical to those observed previously for ERY bound to vacant 70S ribosomes from *Eco* (Supplemental Fig. S1B,E; Dunkle et al. 2010) or *Tth* (Supplemental Fig. S1C,E; Bulkley et al. 2010) in the absence of mRNA and tRNAs. Binding of ERY to the ribosome is largely mediated by the H-bonding between the 23S rRNA residues A2058 and A2059 and the desosamine moiety of the drug, which is pointed in the direction of the PTC (Supplemental Movie S1; Fig. 4). Curiously, in our structure, ERY causes similar reorientation of the nucleotide A2062 of the 23S rRNA (Fig. 4B,C) as in the case with CHL (Fig. 3C,D). However, unlike CHL, which forms H-bond with the A2062 base, ERY does not establish this type of interaction but instead forms van der Waals contact with the A2062/A2503 bases (Supplemental Fig. S3). Moreover, this ERY-induced conformational change of A2062 is observed consistently only in *Tth* 70S ribosomes (current work and Bulkley et al. 2010), but not in the case with *Eco* 70S ribosomes (Dunkle et al. 2010), or *Haloarcula marismortui* 50S ribosomal subunit (Tu et al. 2005). This rearrangement potentially could represent a species-specific response to the binding of a macrolide antibiotic.

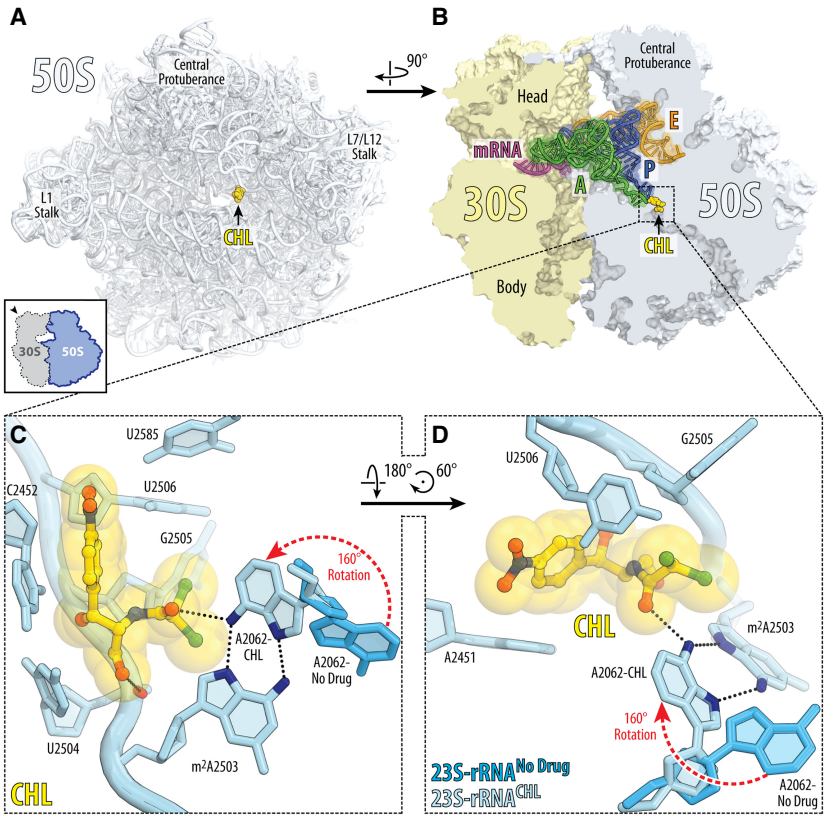

FIGURE 3. Structure of CHL in complex with the 70S ribosome and A-, P-, and E-site tRNAs. (*A*,*B*) Overview of the CHL binding site (yellow) in the *Tth* 70S ribosome viewed from the PTC down the tunnel as indicated by the *inset* (*A*), or as a cross-cut section through the ribosome (*B*). The 30S subunit is shown in light yellow, the 50S subunit is in light blue, the mRNA is in magenta, and the A-, P-, and E-site tRNAs are colored green, dark blue, and orange, respectively. (*C*,*D*) Close-up views of the CHL bound in the PTC. The *E. coli* nucleotide numbering is used. Potential H-bond interactions are indicated with dashed lines. Note that by forming an H-bond with the base of nucleotide A2062 of the 23S rRNA (light blue) CHL causes characteristic rotation of this nucleotide by ~160° to form Hoogsteen base pair with the m^2A2503 of the 23S rRNA (red dashed arrow). *N6* and *N7* atoms of nucleotides A2062 and m^2A2503 are highlighted in dark blue. The unrotated conformation of A2062 observed in the absence of the drug is shown in blue (PDB entry 4Y4P [Polikanov et al. 2015]).

Structural basis for competition between ERY and CHL

The two chemical groups of CHL and ERY that come into close proximity are the dichloroacetic and dimethylamine moieties. The exact rotational orientation of the dichloroacetic group of CHL, which is crucial for our subsequent analysis, was uncertain from the previous structures (Fig. 2A,B). Due to a higher resolution and overall better quality electron density maps that we observed for CHL and ERY (Fig. 2C,F), we were able to unambiguously determine the placement of the dichloroacetic moiety of CHL and provide definitive structural basis for their competition that was previously observed in biochemical assays (Wolfe and Hahn 1965; Vazquez 1966; Pestka 1974).

Superposition of our CHL and ERY structures reveals a direct steric clash between the chlorine atoms of the dichloroacetic moiety of CHL and the dimethylamine of the desosamine sugar of ERY (Fig. 5). Both chemical groups in each of the two drugs are essential for their binding to the ribosome. The dichloroacetic moiety of CHL forms H-bond with the *N6* atom of A2062 of the 23S rRNA (Fig. 5A; Supplemental Movie S1), and mutation of this base to cytidine leads to CHL resistance (Mankin and Garrett 1991; Kloss et al. 1999). Likewise, inability to form H-bonds between desosamine of ERY and the *N1* and *N6* atoms of A2058 and A2059 bases, respectively (Fig. 5B; Supplemental Movie S1), when these bases are mutated to guanines, also causes antibiotic resistance (Vester and Garrett 1987; Sander et al. 1997; Vester and Douthwaite 2001). Therefore, even a minor displacement of any of these groups should lead to disruption of the crucial interaction for either CHL or ERY that would be manifested as competitive binding.

The competition between CHL and ERY was demonstrated biochemically decades ago using ribosomes from several bacterial species, including *E. coli* (Wolfe and Hahn 1965; Vazquez 1966; Pestka 1974). However, such competition has never been tested for the Gram-negative bacterium *T. thermophilus*, which we use as a source of ribosomes in our structural studies. To confirm the ability of macrolides to displace prebound CHL from *Tth* 70S ribosomes, we used competition-binding assay exploiting [^{14}C]-CHL and nonlabeled ERY. In our assays, the macrolide efficiently displaces CHL from both *Eco* (Supplemental Fig. S4A) and *Tth* (Supplemental Fig. S4B) ribosomes in a concentration-dependent manner. Therefore, CHL-ERY competition occurs on *Tth* ribosomes and is likely to be manifested in most of the bacterial species.

Our structural analysis clearly points to a direct steric clash mechanism of competition between CHL and ERY, which was first observed biochemically more than five decades ago. We wonder whether there are any PTC-targeting antibiotics that do not compete (and likely can coexist) with the macrolides on the bacterial ribosome. We believe that finding such inhibitors could potentially lead to the identification of drug pairs exhibiting more efficient and possibly even synergistic antibacterial action.

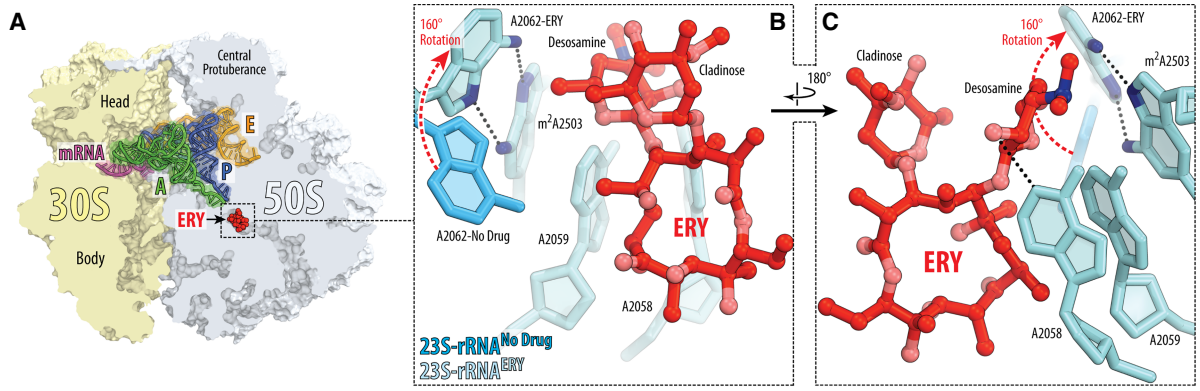

FIGURE 4. Structure of ERY in complex with the 70S ribosome and A- and P-site tRNAs. (*A*) Overview of the ERY binding site (red) in the *T. thermophilus* 70S ribosome viewed as a cross-cut through the peptide exit tunnel. The 30S subunit is shown in light yellow, the 50S subunit is in light blue, the mRNA is magenta, and the A-, P-, and E-site tRNAs are colored in green, dark blue, and orange, respectively. (*B*,*C*) Close-up views of the ERY binding site shown in panel *A*. Potential H-bond interactions are indicated with dashed lines. Note that binding of ERY causes the same characteristic rotation of the nucleotide A2062 to form Hoogsteen base pair with the nucleotide m^2A2503 as observed in the case of CHL (red dashed arrow).

MATERIALS AND METHODS

Materials for biochemical experiments

Nonlabeled CHL and ERY were obtained from MilliporeSigma. Radioactively labeled [^{14}C]-ERY and [^{14}C]-CHL were obtained from MP Biomedicals and Moravek Biochemicals, respectively. Cellulose nitrate filters (type HA, 24-mm diameter, 0.45-µm pore size) were obtained from MilliporeSigma. Scintillation liquid was obtained from Bio-Rad.

Biochemical preparations

Reassociated *Escherichia coli* 70S ribosomes were prepared from K12 strain as previously described (Blaha et al. 2000). Purified ribosomes were stored in a buffer containing 20 mM HEPES-KOH (pH 7.6), 50 mM CH_3COONH_4, 6 mM $Mg(CH_3COO)_2$, and 4 mM β-mercaptoethanol. 70S ribosomes were prepared from *Thermus thermophilus* strain HB8 as described in Polikanov et al. (2014).

Competition-binding assays

Reassociated *Escherichia coli* 70S ribosomes (0.2 µM final concentration) were incubated in buffer A [20 mM HEPES-KOH [pH 7.6], 150 mM $NH_4(CH_3COO)$, 6 mM $Mg(CH_3COO)_2$, 2 mM spermidine, 0.05 mM spermine, and 4 mM β-mercaptoethanol] with [^{14}C]-CHL (150 dpm/pmol) at the appropriate/indicated concentration. After incubation for 10 min at 37°C, the mixture was diluted with 3 mL of cold buffer A and filtered through a 25-mm diameter 0.45-µm pore size nitrocellulose membrane (MilliporeSigma). The filter was immediately washed three times with 3 mL of cold buffer A and bound radioactivity was measured. Next, binding of [^{14}C]-CHL was studied in competition with nonradiolabeled CHL or ERY by maintaining a constant concentration of [^{14}C]-CHL (0.6 µM) and increasing concentrations of a nonradioactive competitor (Karahalios et al. 2006).

In the case of *Thermus thermophilus* 70S ribosomes, the binding competition between CHL and ERY was assessed in the same conditions as the "fragment reaction" described previously (Fernandez-Munoz et al. 1971). Each 25-µL reaction contained 33% (v/v) ethanol, 33 mM Tris-HCl pH 7.5, 270 mM KCl, 13 mM $Mg(CH_3COO)_2$, 4 µM of *Tth* 70S ribosomes and 3 µM of [^{14}C]-CHL (150 dpm/pmol). Increasing concentrations of nonradioactive CHL or ERY were added to the reactions. After incubation at 0°C for 30 min, the ribosomes were precipitated by centrifugation at 14,000*g* for 20 min and radioactivity of CHL in ribosome-free supernatants was measured.

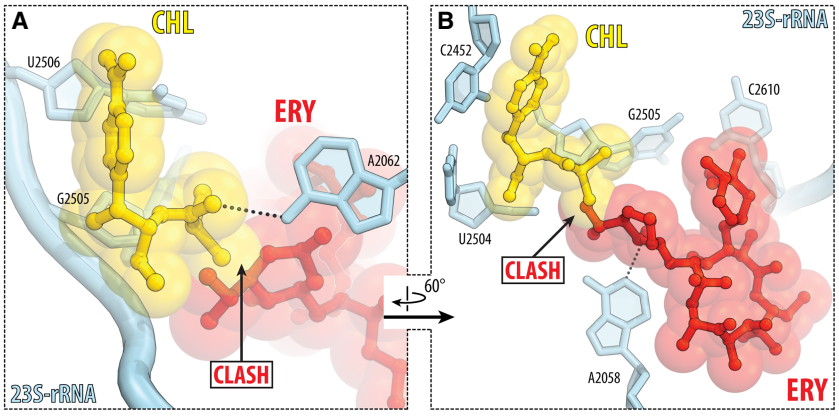

FIGURE 5. Overlap between CHL and ERY binding sites in the 70S ribosome. (*A*,*B*) Two close-up views of the superimposed binding sites for CHL and ERY. The structures were aligned based on the domain V of the 23S rRNA. The coloring of the 23S rRNA and the antibiotics is the same as in Figures 3 and 4. Note that dichloroacetic group of CHL clashes with the dimethylamine group of the desosamine sugar of ERY, rationalizing their mutually exclusive binding to the 70S ribosome.

Crystallographic structure determination

Ribosome complexes with mRNA and tRNAs were formed as described previously (Polikanov et al. 2015). CHL or ERY were added to the preformed ribosome complexes to a final concentration of 250 μM prior to crystallization. All *Tth* 70S ribosome complexes were formed in the buffer containing 5 mM HEPES-KOH (pH 7.6), 50 mM KCl, 10 mM NH_4Cl, and 10 mM $Mg(CH_3COO)_2$, and then crystallized in the buffer containing 100 mM Tris-HCl (pH 7.6), 2.9% (w/v) PEG-20 K, 7%–12% (v/v) MPD, 100–200 mM arginine, 0.5 mM β-mercaptoethanol. Crystals were grown by the vapor diffusion method in sitting drops at 19°C and stabilized as described previously (Polikanov et al. 2015) with CHL or ERY being added to the stabilization buffers (100 μM each). Diffraction data were collected using beamline 24ID-C and 24ID-E at the Advanced Photon Source (Argonne National Laboratory). A complete data set for each ribosome complex was collected using 0.979 Å wavelength at 100 K from multiple regions of the same crystal using 0.3° oscillations. The raw data were integrated and scaled using the XDS software package (Kabsch 2010). All crystals belonged to the primitive orthorhombic space group $P2_12_12_1$ with approximate unit cell dimensions of 210 × 450 × 620 Å and contained two copies of the 70S ribosome per asymmetric unit. Each structure was solved by molecular replacement using PHASER from the CCP4 program suite (McCoy et al. 2007). The search model was generated from the previously published structures of *T. thermophilus* 70S ribosome with bound mRNA and tRNAs (PDB entry 4Y4P from Polikanov et al. [2015]). The initial molecular replacement solutions were refined by rigid body refinement with the ribosome split into multiple domains, followed by positional and individual B-factor refinement using PHENIX (Adams et al. 2010). Noncrystallographic symmetry restraints were applied to four domains of the 30S ribosomal subunit (head, body, spur, helix 44), and four domains of the 50S subunit (body, L1-stalk, L10-stalk, C terminus of the L9 protein).

Atomic models of CHL and ERY were generated from their known chemical structures (Fig. 1A,B) using PRODRG online software (Schüttelkopf and van Aalten 2004), which was also used to generate restraints for energy minimization and refinement based on idealized 3D geometry. Atomic models and restraints were used to fit/refine CHL and ERY into the obtained electron density maps (Fig. 1C,D). The final models of the *Tth* 70S ribosome in complex with mRNA/tRNAs and CHL or ERY were generated by multiple rounds of model building in COOT (Emsley and Cowtan 2004), followed by refinement in PHENIX (Adams et al. 2010). The statistics of data collection and refinement are compiled in Supplemental Table S1. All figures showing atomic models were generated using the PyMol software (www.pymol.org).

DATA DEPOSITION

Coordinates and structure factors were deposited in the RCSB Protein Data Bank with the following accession codes: 6ND5 for the *T. thermophilus* 70S ribosome in complex with chloramphenicol, mRNA, A-, P-, and E-site tRNAs; 6ND6 for the *T. thermophilus* 70S ribosome in complex with erythromycin, mRNA, A-, P-, and E-site tRNAs.

SUPPLEMENTAL MATERIAL

Supplemental material is available for this article.

ACKNOWLEDGMENTS

We thank all members of the G.P.D. and Y.S.P. laboratories for valuable suggestions. We thank Drs. Alexander Mankin and Nora Vazquez-Laslop for important discussions and critical feedback. We thank the staff at NE-CAT beamlines 24ID-C and 24ID-E for help with data collection and freezing of the crystals, especially Drs. Kanagalakhatta Rajashankar, Malcolm Capel, Frank Murphy, Igor Kourinov, Anthony Lynch, Surajit Banerjee, David Neau, Jonathan Schuermann, Narayanasami Sukumar, James Withrow, Kay Perry, and Cyndi Salbego. This work is based upon research conducted at the Northeastern Collaborative Access Team beamlines, which are funded by the National Institute of General Medical Sciences from the National Institutes of Health (P41 GM103403 to NE-CAT). The Pilatus 6M detector on 24ID-C beamline is funded by a NIH-ORIP HEI (S10 RR029205 to NE-CAT). The Eiger 16M detector on 24ID-E beamline is funded by a NIH-ORIP HEI grant (S10 OD021527 to NE-CAT). This research used resources of the Advanced Photon Source, a U.S. Department of Energy (DOE) Office of Science User Facility operated for the DOE Office of Science by Argonne National Laboratory under contract no. DE-AC02-06CH11357. This work was supported by Illinois State startup funds (to Y.S.P.) and National Institutes of Health (R21-AI137584 to Y.S.P.); and University of Patras funds (to G.P.D.).

Author contributions: M.S.S. performed competition-binding assays using *T. thermophilus* 70S ribosomes; E.P., A.B., and M. G.K. performed competition-binding assays using *E. coli* 70S ribosomes; Y.S.P., M.S.S., and C.W.C. designed and performed X-ray crystallography experiments; G.P.D. and Y.S.P. supervised the experiments. All authors interpreted the results. M.S.S., G.P. D., and Y.S.P. wrote the manuscript.

Received October 16, 2018; accepted January 28, 2019.

REFERENCES

Adams PD, Afonine PV, Bunkóczi G, Chen VB, Davis IW, Echols N, Headd JJ, Hung LW, Kapral GJ, Grosse-Kunstleve RW, et al. 2010. *PHENIX*: a comprehensive Python-based system for macromolecular structure solution. *Acta Crystallogr D Biol Crystallogr* **66:** 213–221. doi:10.1107/S0907444909052925

Almutairi MM, Svetlov MS, Hansen DA, Khabibullina NF, Klepacki D, Kang HY, Sherman DH, Vázquez-Laslop N, Polikanov YS, Mankin AS. 2017. Co-produced natural ketolides methymycin and pikromycin inhibit bacterial growth by preventing synthesis of a limited number of proteins. *Nucleic Acids Res* **45:** 9573–9582. doi:10.1093/nar/gkx673

Blaha G, Stelzl U, Spahn CM, Agrawal RK, Frank J, Nierhaus KH. 2000. Preparation of functional ribosomal complexes and effect of buffer conditions on tRNA positions observed by cryoelectron microscopy. *Methods Enzymol* **317:** 292–309. doi:10.1016/S0076-6879(00)17021-1

Bulkley D, Innis CA, Blaha G, Steitz TA. 2010. Revisiting the structures of several antibiotics bound to the bacterial ribosome. *Proc Natl Acad Sci* **107:** 17158–17163. doi:10.1073/pnas.1008685107

Dunkle JA, Xiong L, Mankin AS, Cate JH. 2010. Structures of the *Escherichia coli* ribosome with antibiotics bound near the peptidyl transferase center explain spectra of drug action. *Proc Natl Acad Sci* **107:** 17152–17157. doi:10.1073/pnas.1007988107

Emsley P, Cowtan K. 2004. *Coot*: model-building tools for molecular graphics. *Acta Crystallogr D Biol Crystallogr* **60:** 2126–2132. doi:10.1107/S0907444904019158

Fernandez-Munoz R, Monro RE, Torres-Pinedo R, Vazquez D. 1971. Substrate- and antibiotic-binding sites at the peptidyl-transferase centre of *Escherichia coli* ribosomes. Studies on the chloramphenicol, lincomycin and erythromycin sites. *Eur J Biochem* **23:** 185–193. doi:10.1111/j.1432-1033.1971.tb01607.x

Hansen JL, Moore PB, Steitz TA. 2003. Structures of five antibiotics bound at the peptidyl transferase center of the large ribosomal subunit. *J Mol Biol* **330:** 1061–1075. doi:10.1016/S0022-2836(03)00668-5

Kabsch W. 2010. Xds. *Acta Crystallogr D Biol Crystallogr* **66:** 125–132. doi:10.1107/S0907444909047337

Karahalios P, Kalpaxis DL, Fu H, Katz L, Wilson DN, Dinos GP. 2006. On the mechanism of action of 9-*O*-arylalkyloxime derivatives of 6-*O*-mycaminosyltylonolide, a new class of 16-membered macrolide antibiotics. *Mol Pharmacol* **70:** 1271–1280. doi:10.1124/mol.106.026567

Kloss P, Xiong L, Shinabarger DL, Mankin AS. 1999. Resistance mutations in 23S rRNA identify the site of action of the protein synthesis inhibitor linezolid in the ribosomal peptidyl transferase center. *J Mol Biol* **294:** 93–101. doi:10.1006/jmbi.1999.3247

Lin J, Zhou D, Steitz TA, Polikanov YS, Gagnon MG. 2018. Ribosome-targeting antibiotics: modes of action, mechanisms of resistance, and implications for drug design. *Annu Rev Biochem* **87:** 451–478. doi:10.1146/annurev-biochem-062917-011942

Mankin AS, Garrett RA. 1991. Chloramphenicol resistance mutations in the single 23S rRNA gene of the archaeon *Halobacterium halobium*. *J Bacteriol* **173:** 3559–3563. doi:10.1128/jb.173.11.3559-3563.1991

McCoy AJ, Grosse-Kunstleve RW, Adams PD, Winn MD, Storoni LC, Read RJ. 2007. *Phaser* crystallographic software. *J Appl Crystallogr* **40:** 658–674. doi:10.1107/S0021889807021206

Metelev M, Osterman IA, Ghilarov D, Khabibullina NF, Yakimov A, Shabalin K, Utkina I, Travin DY, Komarova ES, Serebryakova M, et al. 2017. Klebsazolicin inhibits 70S ribosome by obstructing the peptide exit tunnel. *Nat Chem Biol* **13:** 1129–1136. doi:10.1038/nchembio.2462

Osterman IA, Khabibullina NF, Komarova ES, Kasatsky P, Kartsev VG, Bogdanov AA, Dontsova OA, Konevega AL, Sergiev PV, Polikanov YS. 2017. Madumycin II inhibits peptide bond formation by forcing the peptidyl transferase center into an inactive state. *Nucleic Acids Res* **45:** 7507–7514. doi:10.1093/nar/gkx413

Pantel L, Florin T, Dobosz-Bartoszek M, Racine E, Sarciaux M, Serri M, Houard J, Campagne JM, de Figueiredo RM, Midrier C, et al. 2018. Odilorhabdins, antibacterial agents that cause miscoding by binding at a new ribosomal site. *Mol Cell* **70:** 83–94. doi:10.1016/j.molcel.2018.03.001

Pestka S. 1974. Antibiotics as probes of ribosome structure: binding of chloramphenicol and erythromycin to polyribosomes; effect of other antibiotics. *Antimicrob Agents Chemother* **5:** 255–267. doi:10.1128/AAC.5.3.255

Polikanov YS, Steitz TA, Innis CA. 2014. A proton wire to couple aminoacyl-tRNA accommodation and peptide-bond formation on the ribosome. *Nat Struct Mol Biol* **21:** 787–793. doi:10.1038/nsmb.2871

Polikanov YS, Melnikov SV, Söll D, Steitz TA. 2015. Structural insights into the role of rRNA modifications in protein synthesis and ribosome assembly. *Nat Struct Mol Biol* **22:** 342–344. doi:10.1038/nsmb.2992

Polikanov YS, Aleksashin NA, Beckert B, Wilson DN. 2018. The mechanisms of action of ribosome-targeting peptide antibiotics. *Front Mol Biosci* **5:** 48. doi:10.3389/fmolb.2018.00048

Sander P, Prammananan T, Meier A, Frischkorn K, Böttger EC. 1997. The role of ribosomal RNAs in macrolide resistance. *Mol Microbiol* **26:** 469–480. doi:10.1046/j.1365-2958.1997.5811946.x

Schlünzen F, Zarivach R, Harms J, Bashan A, Tocilj A, Albrecht R, Yonath A, Franceschi F. 2001. Structural basis for the interaction of antibiotics with the peptidyl transferase centre in eubacteria. *Nature* **413:** 814–821. doi:10.1038/35101544

Schüttelkopf AW, van Aalten DM. 2004. *PRODRG*: a tool for high-throughput crystallography of protein-ligand complexes. *Acta Crystallogr D Biol Crystallogr* **60:** 1355–1363. doi:10.1107/S0907444904011679

Tereshchenkov AG, Dobosz-Bartoszek M, Osterman IA, Marks J, Sergeeva VA, Kasatsky P, Komarova ES, Stavrianidi AN, Rodin IA, Konevega AL, et al. 2018. Binding and action of amino acid analogs of chloramphenicol upon the bacterial ribosome. *J Mol Biol* **430:** 842–852. doi:10.1016/j.jmb.2018.01.016

Tu D, Blaha G, Moore PB, Steitz TA. 2005. Structures of MLSBK antibiotics bound to mutated large ribosomal subunits provide a structural explanation for resistance. *Cell* **121:** 257–270. doi:10.1016/j.cell.2005.02.005

Van Boeckel TP, Gandra S, Ashok A, Caudron Q, Grenfell BT, Levin SA, Laxminarayan R. 2014. Global antibiotic consumption 2000 to 2010: an analysis of national pharmaceutical sales data. *Lancet Infect Dis* **14:** 742–750. doi:10.1016/S1473-3099(14)70780-7

Vazquez D. 1966. Binding of chloramphenicol to ribosomes. The effect of a number of antibiotics. *Biochim Biophys Acta* **114:** 277–288. doi:10.1016/0005-2787(66)90309-1

Vester B, Douthwaite S. 2001. Macrolide resistance conferred by base substitutions in 23S rRNA. *Antimicrob Agents Chemother* **45:** 1–12. doi:10.1128/AAC.45.1.1-12.2001

Vester B, Garrett RA. 1987. A plasmid-coded and site-directed mutation in *Escherichia coli* 23S RNA that confers resistance to erythromycin: implications for the mechanism of action of erythromycin. *Biochimie* **69:** 891–900. doi:10.1016/0300-9084(87)90217-3

Wolfe AD, Hahn FE. 1965. Mode of action of chloramphenicol. IX. Effects of chloramphenicol upon a ribosomal amino acid polymerization system and its binding to bacterial ribosome. *Biochim Biophys Acta* **95:** 146–155. doi:10.1016/0005-2787(65)90219-4